Electrogenerated chemiluminescence of luminol in neutral and alkaline aqueous solutions on a silver nanoparticle self-assembled gold electrode

ARTICLE *in* LUMINESCENCE · JANUARY 2007

Impact Factor: 1.52 · DOI: 10.1002/bio.924 · Source: PubMed

Luminescence 2007; 22: 35–45
Published online 27 July 2006 in Wiley InterScience (www.interscience.wiley.com) DOI: 10.1002/bio.924 *ORIGINAL RESEARCH*

Electrogenerated chemiluminescence of luminol in neutral and alkaline aqueous solutions on a silver nanoparticle self-assembled gold electrode

Cheng-Ming Wang and Hua Cui*

Department of Chemistry, University of Science and Technology of China, Hefei, Anhui 230026, People's Republic of China

Received 18 January 2006; revised 10 April 2006; accepted 21 April 2006

ABSTRACT: The electrochemiluminescence (ECL) behaviour of luminol on a silver nanoparticle self-assembled gold electrode in neutral and alkaline solutions was investigated using conventional cyclic voltammetry (CV). The silver nanoparticle self-assembled gold electrode exhibited excellent ECL properties for the luminol ECL system. In neutral solutions, four ECL peaks (ECL-1–ECL-4) were observed at 0.73, 1.15, –0.46 and –1.35 V (vs. SCE), respectively. The intensities of these peaks were enhanced significantly compared with those on a bulk gold electrode and a gold nanoparticle self-assembled gold electrode. It was found that ECL-1 and ECL-2 on a silver nanoparticle-modified electrode were about 1000 and 1770 times stronger than those on a bare Au electrode and were about 17 and 15 times stronger than those on a gold nanoparticle-modified electrode, respectively. In alkaline solutions, four ECL peaks were also observed that were much stronger than those in neutral solutions, and ECL-1 and ECL-2 were enhanced by about three orders and one order of magnitude compared with those on a bare Au electrode and on a gold nanoparticle self-assembled electrode, respectively. Moreover, the silver nanoparticle-modified electrode exhibited good stability and reproducibility for luminol ECL. These peaks were found to depend on a number of factors, including silver nanoparticles on the surface of the modified electrode, potential scan direction, scan rate, scan range, the presence of O_2 or N_2, pH values, the concentrations of NaBr and luminol, and buffer solutions. The emitter of the ECL was confirmed as 3-aminophthalate by analysing the CL spectra. The surface state of the silver nanoparticle self-assembled electrode was characterized by scanning electron microscopy (SEM) and the interface property of the electrode was studied by electrochemical impedance spectroscopy (EIS). A mechanism for the formation of these ECL peaks is proposed. The results demonstrate that luminol has excellent ECL properties, such as strong ECL intensity and good reproducibility on a silver nanoparticle-modified gold electrode, in both neutral and alkaline solutions, which is of great potential in analytical applications. Copyright © 2006 John Wiley & Sons, Ltd.

KEYWORDS: electrochemiluminescence; CV; luminol; silver nanoparticle self-assembled gold electrode; effect factors; mechanism

INTRODUCTION

Electrogenerated chemiluminescence (ECL) has become an important and valuable detection method in analytical chemistry (1) due to its promising advantages, such as simplicity, rapidity, high sensitivity and easy controllability. Luminol is one of the most widely used ECL reagents. Luminol ECL behaviour has been studied at various electrodes, such as carbon (2), glassy carbon (3), platinum (3), paraffin-impregnated graphite (4), oxide-coated aluminium (5), indium–tin oxide (ITO) (6), gold (7) and copper (8), and several modified electrodes, such as cobalt (II) hexacyanoferrate (9), ferrocenylalkanethiol (10) and nickel phthalocyanine (11). It was found that luminol ECL depended on the applied potential, electrode material and surface state of the electrode. Previous work revealed that strong luminol ECL may be obtained by optimizing the composition and surface structure of the electrode. For this purpose, a gold nanoparticle self-assembled gold electrode was used to study the ECL behaviours of luminol in neutral and alkaline solutions, and exhibited remarkable ECL properties (12).

It is well known that silver nanoparticles prepared by adding $AgNO_3$ to $NaBH_4$ are highly mono-dispersed. Silver nanoparticles exhibit excellent catalytic, electrocatalytic and chemical activities (13–18) due to surface and microscale effects and low electron-transfer resistivity. As silver can be more easily oxidized than gold (19) and some charge transfer toward the surface takes place according to the sequence silver > gold (20), certain electrocatalytic reactions occur more rapidly with silver nanoparticles as a catalyst than with gold nanoparticles. Moreover, silver and gold mixed colloids can form a favourable aggregation state and significantly increase the surface-enhanced Raman scattering (SERS) activity compared with single silver and gold colloids

*Correspondence to: H. Cui, Department of Chemistry, University of Science and Technology of China, Hefei, Anhui 230026, People's Republic of China.
E-mail: hcui@ustc.edu.cn

Contract/grant sponsor: National Natural Science Foundation of China; Contract/grant number: 29875025 and 20375037.
Contract/grant sponsor: Chinese Academy of Sciences.

(21). Inhibition of the silver-catalysed reaction caused by insoluble silver salts at the surface can be avoided if a small amount of gold is deposited on silver (19). Therefore, the nanosilver-modified gold electrode may offer better ECL properties than a nanogold-modified gold electrode.

In this work, a silver nanoparticle self-assembled gold electrode was used to study luminol ECL in neutral and alkaline solutions under cyclic voltammetric conditions. It was found that luminol exhibited outstanding ECL properties on this type of electrode. Compared with a bulk gold electrode and a gold nanoparticle self-assembled gold electrode, the intensities of ECL peaks were greatly enhanced in both neutral and alkaline aqueous solutions. The effects of various factors, such as potential scan direction, potential scan rate, potential scan range, the presence of N_2 and O_2, pH, concentrations of NaBr and luminol, and buffer solutions on ECL peaks, were also examined. A possible mechanism for each luminol ECL peak on a silver nanoparticle self-assembled electrode is proposed.

EXPERIMENTAL

Chemicals and reagents

Luminol was obtained from Merck (Germany) and used without any further purification. A 1.0×10^{-2} mol/L stock solution of luminol was prepared by dissolving luminol in 0.1 mol/L sodium hydroxide solution. Working solutions of luminol were prepared by diluting the stock solution. Silver nitrate was obtained from Shanghai Reagent (Shanghai, China). Supporting electrolyte was composed of 0.1 mol/L NaBr solution and 0.1 mol/L phosphate buffer solution (PBS). PBSs with various pH values were prepared by mixing 0.1 mol/L stock standard solutions of K_2HPO_4 and KH_2PO_4, or by adjusting the pH with 0.1 mol/L H_3PO_4 solution or with NaOH. Nitrogen and oxygen of 99.999% purity were used. All other reagents were of analytical grade, and redistilled water was used throughout.

Synthesis and characterization of silver nanoparticles

Silver colloids were prepared by adding a 50 mL portion of 1×10^{-3} mol/L $AgNO_3$ aqueous solution dropwise to 150 mL 2×10^{-3} mol/L $NaBH_4$ aqueous solution, with vigorous stirring simultaneously. The resulting yellow silver colloids were characterized by transmission electron microscopy (TEM) (Hitachi H-800, Japan) and UV-visible spectra (Shimadzu UV-2401 PCS spectrophotometer, Japan). Statistical analysis of TEM data revealed that the average diameter of the silver colloids was about 20 ± 5 nm. The UV-visible spectra exhibited a well-developed surface plasmon absorption peak at about 396 nm.

Fabrication of silver nanoparticle self-assembled gold electrode

Cysteine has been chosen to immobilize silver nanoparticles on a bulk gold electrode as it has two functional groups, $-NH_2$ and $-SH$. The bulk gold electrode was polished with abrasive paper, rinsed with ethanol and redistilled water to remove the remaining traces and dried with filter paper. Then, the bulk gold electrode was cycled at 0–1.5 V (vs. SCE) in 0.5 mol/L sulphuric acid at a scan rate of 40 mV/s. This potential cycling was continued until a reproducible voltammogram for gold oxide/reduction components was obtained, indicating that a clean surface of gold electrode was obtained. The electrode was cleaned again in an ultrasonic bath and rinsed with redistilled water. The cleaned electrode was dipped into 0.1 mol/L cysteine aqueous solution for 2 h at room temperature in darkness to form a monolayer of cysteine. The resulting monolayer modified electrode was first rinsed with redistilled water and then soaked in redistilled water for 10 h to remove the physically adsorbed cysteine, then it was immersed in the colloidal silver for another 24 h at 4°C. After these treatments, silver nanoparticles were assembled on the gold electrode. Finally, the silver nanoparticle self-assembled electrode was dipped into redistilled water at 4°C for storage. The surface state of the silver nanoparticle self-assembled electrode was characterized by scanning electron microscopy (SEM; JEOL JSM-6700F, Japan).

a.c. impedance measurements

A model CHI 760B electrochemical working station (Chenhua Inc., Shanghai) was used to record electrochemical impedance spectroscopy (EIS). The a.c. impedance measurements were carried out at an amplitude of 5 mV in the frequency range 100 000–0.01 Hz. Complex impedance plots were obtained at 0.355 V with a $[Fe(CN)_6]^{3-}/[Fe(CN)_6]^{4-}$ pair acting as a probe.

Electrochemical and ECL measurements

ECL and electrochemical (EC) measurements were performed by a home-made ECL/EC system, including a model CHI832 electrochemical working station (Chenhua Inc., Shanghai; i.e. the Chinese distributor of CH Instruments Inc., Austin, TX), an H-type electrochemical cell (self-designed), a model 1P21 photomultiplier tube (PMT) (Beijing, China), a model GD-1 luminometer (Xi'an, China), and a computer. The H-type ECL cell was constructed as described previously (4, 7). A gold foil measuring 6.5×6.8 mm^2 modified with silver nanoparticles served as the working electrode, a

DOI: 10.1002/bio

platinum wire as the counter-electrode, and a silver wire as the quasi-reference electrode (AgQRE). A silver quasi-reference electrode was used for simplicity for cell construction and quick potential response. Although the potential of the AgQRE was found to be essentially stable during the experiment, measurements of $\Delta E = E_{Ag/Ag+} - E_{SCE}$ in different solutions were taken for potential calibrations.

During all experiments, 2.0 mL sample solution was filled in the working compartment and 2.0 mL blank solution without luminol was filled in the auxiliary compartment of the ECL cell. When the suitable potential was applied to the working electrode, an ECL signal was generated. The curves of current vs. applied potential ($i - E$) and the curves of ECL intensity vs. applied potential ($I_{ECL} - E$) were recorded simultaneously. Under a nitrogen or an oxygen atmosphere, nitrogen or oxygen was bubbled through the solutions for 15 min in both compartments of the cell, and the flow was maintained over the solution during experiments. Unless otherwise stated, all experiments were carried out at ambient room temperature and the silver nanoparticle self-assembled gold electrode was stored in redistilled water at all times except during each measurement.

ECL spectra measurements

A RF-5301 PCS spectrofluorophotometer (Shimadzu, Japan) was used to record the CL spectra of various ECL peaks at different potentials under cyclic voltammetry conditions. The time for recording each ECL spectrum was 3 s, and the adopted potential ranges for the measurement of ECL-1, ECL-2, ECL-3, ECL-4 and ECL-5 were 0.65 to 0.77, 1.06 to 1.18, –0.42 to –0.54, –1.43 to –1.31 and 1.42 to 1.54 V, respectively. In each potential range, the ECL intensity did not change significantly with the potential. Moreover, CL spectra of the five ECL peaks at different potentials were also measured by inserting filters with different wavelengths and the results were consistent with those obtained using the spectrofluorophotometer.

RESULTS AND DISCUSSION

Characterization of the surface state of the silver nanoparticle self-assembled electrode by SEM

The surface states of a bare gold electrode (A) and a silver nanoparticle self-assembled gold electrode (B) characterized by SEM are shown in Fig. 1. As seen in these images, the surface of the bare gold electrode was smooth and uniform without any holes or cavities. The silver nanoparticles dispersed evenly and formed almost a continuous monolayer on the surface of the electrode. The statistical average size (~20 ± 2 nm) of silver nanoparticles on the surface of the modified electrode was almost consistent with the average size (~20 ± 5 nm) of silver colloids. The result indicated the formation of a silver nanoparticle self-assembled electrode.

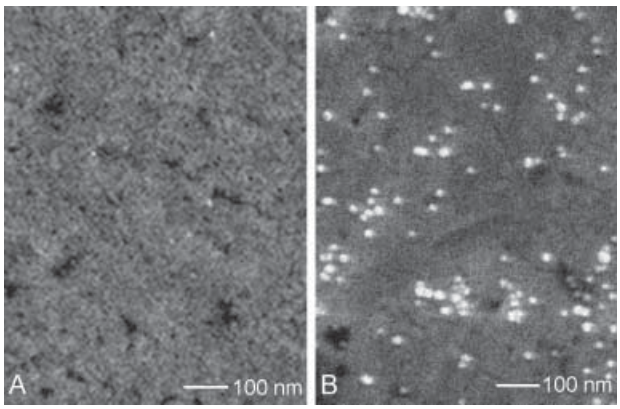

Figure 1. SEM images of a bare gold electrode (A) and a silver nanoparticle self-assembled gold electrode (B).

Electrochemical impedance spectra for three types of electrode

Electrochemical impedance spectroscopy (EIS) is an effective tool for studying the interface properties of surface-modified electrodes (22–24). To better understand the properties of silver self-assembly film in the ECL process, EISs were recorded as shown in Fig. 2. The impedance spectroscopy result for the bare gold electrode was a semicircle in all frequency domains, indicating that the process was controlled only by electron transfer. When gold or silver nanoparticles were modified on the gold electrode, the impedance spectra consisted of a semicircle at high a.c. modulation frequencies and a line at low a.c. modulation frequencies, demonstrating that the process on gold or silver nanoparticle-modified electrode was controlled by electron transfer at high frequencies and by diffusion at low frequencies. The diameter of the Nyquist circle on the electrode decreased in the order: bare gold electrode > gold nanoparticle-modified gold electrode > silver nanoparticle-modified gold electrode, indicating that the electron transfer on the silver nanoparticle-modified gold electrode was the fastest among the three electrodes.

Electrochemical and ECL behaviour of luminol in neutral solution under air-saturated conditions

Cyclic voltammograms (CVs) and $I_{ECL} - E$ curves of 10^{-4} mol/L luminol in neutral solution containing 0.1 mol/L PBS and 0.1 mol/L NaBr on a silver nanoparticle self-assembled gold electrode, on a gold nanoparticle self-assembled gold electrode and on a bulk

DOI: 10.1002/bio

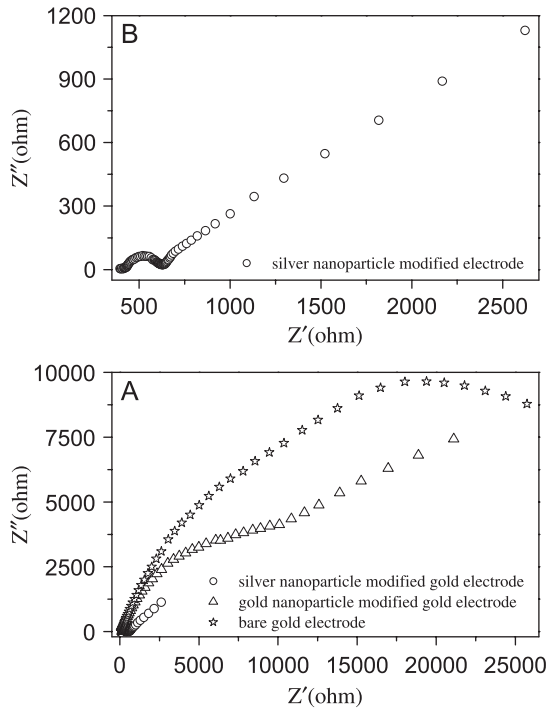

Figure 2. Electrochemical impedance spectra for a bare gold electrode (☆), a gold nanoparticle-modified gold electrode (△) and a silver nanoparticle-modified gold electrode (○). $K_3Fe(CN)_6$, 10^{-3} mol/L; KCl, 0.05 mol/L. The pH of the electrolyte is 7.0.

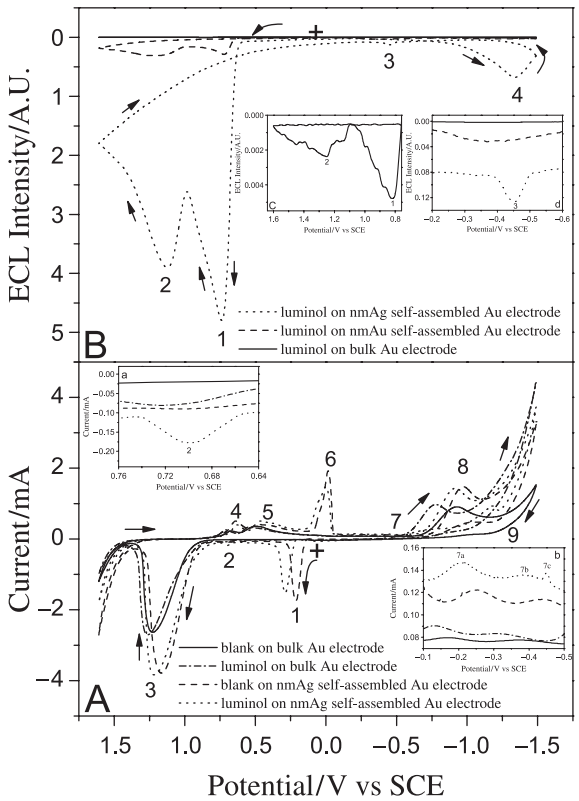

Figure 3. (A) CV curves on a bulk gold electrode in blank solution (solid line) and in sample solution (dashed/dotted line) and on a silver nanoparticle self-assembled gold electrode in blank solution (dashed line) and in sample solution (dotted line). (B) $I_{ECL} - E$ curves of luminol on a silver nanoparticle self-assembled gold electrode (dotted line), on a gold nanoparticle self-assembled gold electrode (dashed line) and on a bulk gold electrode (solid line) under an air-saturated atmosphere. pH 7.0 PBS, 0.1 mol/L; NaBr, 0.1 mol/L; luminol, 1×10^{-4} mol/L; scan rate, 40 mV/s; high voltage, –550 V. Inset (a) shows the enlarged cvp2 from 0.64 to 0.76 V; inset (b) shows the enlarged cvp7 from –0.10 to –0.50 V; inset (c) shows the enlarged ECL-1 and ECL-2 from 0.76 to 1.61 V on a bulk gold electrode; and inset (d) shows the enlarged ECL-3 from –0.20 to –0.60 V.

gold electrode under air-saturated conditions are shown in Fig. 3.

Three anodic cyclic voltammetric peaks (cvp1, cvp2 and cvp3) were observed at 0.29, 0.70 and 1.17 V (vs. SCE), respectively, on the positive scan (Fig. 3A). Upon reversal of the potential scan from 1.61 V, five cathodic peaks (cvp4, cvp5, cvp6, cvp7, cvp8) were found at 0.63, 0.47, 0.002, −0.45 and −0.92 V, respectively. Another anodic peak (cvp9) occurred at –1.23 V in the positive scan from –1.49 V. Cvp1 and cvp6 were attributed to the oxidation and reduction of silver nanoparticles and silver ions, because cvp1 and cvp6 were only observed on a silver nanoparticle self-assembled electrode and also occurred in the blank solution. Cvp2 disappeared in the blank solution without luminol and corresponded to the oxidation of luminol to luminol radical anion (12). Cvp3 and cvp4 observed both on a bulk gold electrode and on a silver nanoparticle-modified electrode were attributed to the oxidation and reduction of gold, as they appeared in blank solution without luminol (25). Cvp3 was probably also related to the oxidation of Br^- (4) because cvp3 was much weaker in $NaNO_3$ than in NaBr (Fig. 4A). However, it was difficult to distinguish the oxidation peak of Br^- from that of gold under this condition. When NaBr was displaced by NaI and NaCl as the electrolyte, the oxidation peak of I^- appeared at a more negative potential, while the oxidation peak of Cl^- appeared at a more positive potential, which separated from that of gold and showed indirect evidence for the oxidation of Br^-. Cvp5 was hypothesized to be the reduction of an oxidation product of Br^-, because the peak disappeared when $NaNO_3$ or KI were used as the electrolyte and when the switching potential was below 0.91 V (before cvp3). Cvp7a and cvp7b were due to the reduction of the dissolved oxygen in solution to OOH^- and OH^-, according to our previous studies (3, 7). It was possible that cvp7c was related to nanosilver because it only occurred on a nanosilver-modified electrode. Cvp8 was connected with the reduction of PO_4^{3-}, which was observed in PBS but not in boracic acid buffer solution (12) or citric acid–NaOH buffer solution. Cvp9 was attributed to nanosilver and a redox product of Br^- because it appeared only on a silver nanoparticle

DOI: 10.1002/bio

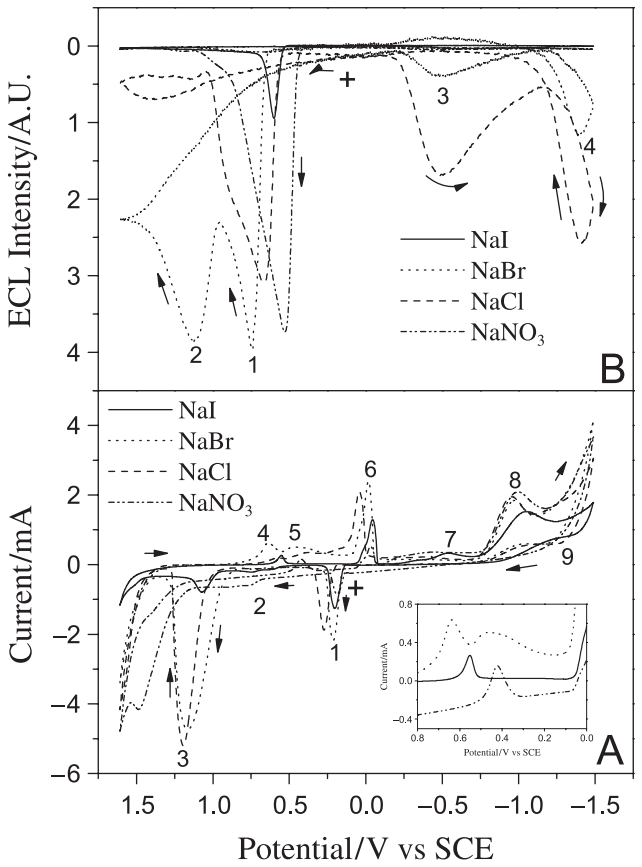

Figure 4. CV (A) and $I_{ECL} - E$ (B) curves of luminol on a silver nanoparticle self-assembled gold electrode in different electrolytes. Electrolytes: 0.1 mol/L $NaNO_3$ (dash/dot/dot line), 0.1 mol/L NaCl (dashed line), 0.1 mol/L NaBr (dotted line) and 1×10^{-3} mol/L NaI (solid line). pH 7.0 PBS, 0.1 mol/L; luminol, 1×10^{-4} mol/L; scan rate, 40 mV/s; high voltage, –550 V. The inset shows the enlarged cvp4 and cvp5 in NaI, NaBr and $NaNO_3$ solutions from 0.80 to 0.00 V.

self-assembled electrode (Fig. 3A) and disappeared when $NaNO_3$ was substituted for NaBr. The onset of H_2 was at about –1.49 V (4, 7).

$I_{ECL} - E$ curves on a silver nanoparticle self-assembled electrode are shown in Fig. 3B. On the positive scan, ECL-1 and ECL-2, corresponding to two anodic voltammetric peaks (cvp2 and cvp3), were observed at 0.73 and 1.15 V, respectively. On the reverse scan, corresponding to cathodic voltammetric peak cvp7 and the potential of H_2 onset, ECL-3 and ECL-4 were obtained at –0.46 and –1.35 V, respectively. Compared with a bare bulk gold electrode, ECL-1 and ECL-2 on a silver nanoparticle self-assembled electrode were enhanced by about 1000 and 1770 times, and shifted negatively by 0.09 and 0.11 V, respectively. The negative shifts were attributed to nanosilver catalysing the oxidation of luminol, because peak currents of cvp2 and cvp3 increased significantly and the positions of cvp2 and cvp3 shifted negatively. ECL-3 and ECL-4 could be observed clearly on a silver nanoparticle self-assembled electrode but not on a bulk gold electrode, implying that nanosilver and its corresponding ions were also crucial to the generation of ECL-3 and ECL-4. Moreover, ECL-1, ECL-2, ECL-3 and ECL-4 on a silver nanoparticle self-assembled electrode were 17, 15, 13 and 30 times stronger, respectively, than those on a gold nanoparticle self-assembled electrode. The results indicate that a silver nanoparticle-modified electrode can provide stronger ECL for luminol system than a gold nanoparticle-modified electrode.

ECL behaviour of luminol in different electrolytes

The ECL behaviour of 10^{-4} mol/L luminol in neutral solution under air-saturated conditions on a silver nanoparticle self-assembled gold electrode was examined in 0.1 mol/L NaCl, NaBr, $NaNO_3$ solution and 1×10^{-3} mol/L NaI solution (since the solubility of NaI is poor, a lower concentration of NaI was used), respectively, in the presence of 0.1 mol/L PBS (pH = 7.0). As shown in the $I_{ECL} - E$ curves (Fig. 4B), the intensity and number of ECL peaks were related to the electrolytes. ECL-1 appeared in all the four electrolytes and the intensity of ECL-1 in NaBr was almost equal to that in $NaNO_3$. For halide ions (X^-), the magnitude of ECL-1 was in the order: $Br^- > Cl^- > I^-$, which was consistent with previous work (26). The results demonstrated that halide ions were not necessary for the formation of ECL-1, but influenced the intensity of ECL-1. ECL-2 occurred in NaBr and NaCl and disappeared in $NaNO_3$, indicating that ECL-2 was related to halide ions. ECL-2 in NaI solution was not detectable, which may be due to much lower concentration of NaI than that of NaBr and NaCl. At the potential, halide ions, for example Br^-, might be oxidized to BrO^- (4, 12), thus BrO^- was one of the reacting species in the ECL-2 reaction. The intensity of ECL-3 in the sodium halide solutions was in the order: $Cl^- > Br^- > I^-$, and ECL-3 was almost undetectable in $NaNO_3$, implying that XO^- generated at positive scan was also involved in the ECL-3 reaction. The intensity of ECL-4 in NaCl was stronger than that in NaBr, and ECL-4 was almost undetectable in NaI and $NaNO_3$. Therefore, it is deduced that ECL-4 correlated to the redox product of X^- during a positive potential scan and corresponding reverse scan. X^- during a positive potential scan was oxidized to XO^-, which was probably reduced to X_2 at such a negative potential (ECL-4). Substituting NaI for NaBr and adding starch to the solution, the colour of the solution changed to blue at about –0.20 V, confirming that I_2 was formed. Thus, XO^- generated at positive scan was indeed converted to X_2, which took part in the ECL-4 reaction. The intensity of ECL-4 in the sodium halide solutions decreased in the order: $Cl^- > Br^- > I^-$, which is in good agreement with the oxidation ability of X_2 ($Cl_2 > Br_2 > I_2$).

DOI: 10.1002/bio

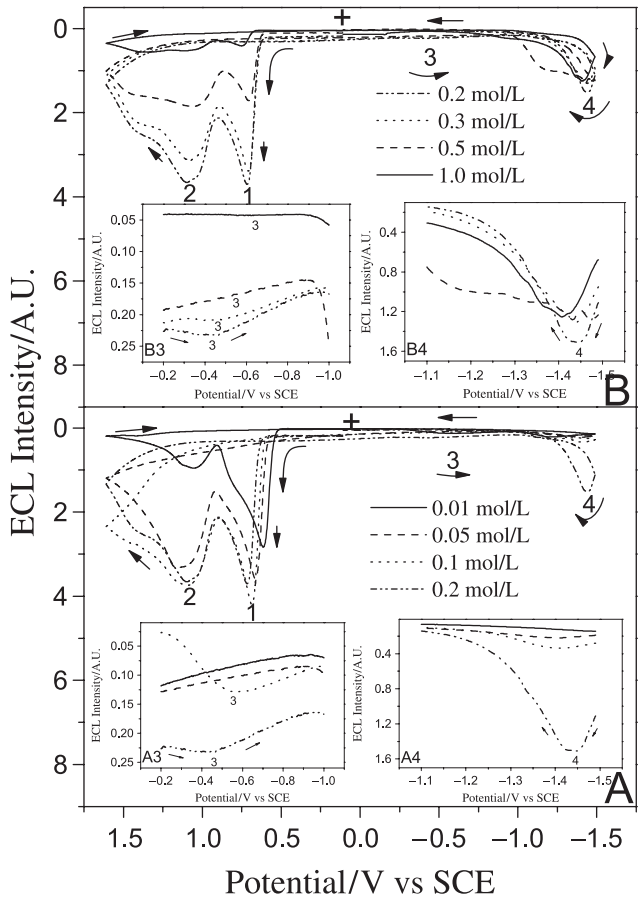

Figure 5. Effect of NaBr concentrations on $I_{ECL} - E$ curves on a silver nanoparticle self-assembled gold electrode. pH 7.0 PBS, 0.1 mol/L; luminol, 1×10^{-4} mol/L; scan rate, 40 mV/s; high voltage, –550 V. Insets (A3) and (B3) show the enlarged ECL-3 from –0.20 to –1.00 V; insets (A4) and (B4) show the enlarged ECL-4 from –1.49 to –1.10 V.

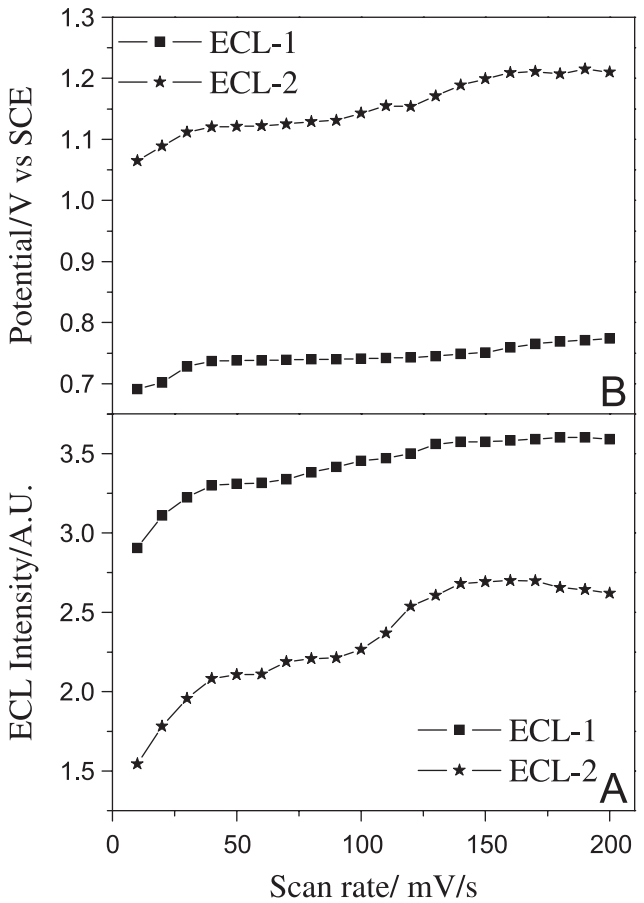

Figure 6. Effect of scan rates on the ECL intensity (A) and peak potential (B) on a silver nanoparticle self-assembled gold electrode. pH 7.0 PBS, 0.1 mol/L; NaBr, 0.1 mol/L; luminol, 1×10^{-4} mol/L; high voltage, –500 V.

The effects of NaBr concentrations on luminol ECL signals were investigated in the range 0.01–1 mol/L, as shown in Fig. 5. From 0.01 to 0.1 mol/L, ECL-1, ECL-2, ECL-3 and ECL-4 increased significantly. The enhancement of ECL-1 could be due to an increase in ion intensity, whereas the enhancement of ECL-2–ECL-4 may be because ECL-2–ECL-4 were related to the redox products of Br^- (4, 12). However, from 0.2 to 1 mol/L, ECL-1, ECL-2, ECL-3 and ECL-4 decreased significantly, which may be due to the strong quenching effect caused by heavier halide ions at higher concentrations (4).

ECL behaviour of luminol under different atmospheres

The ECL behaviour of luminol under different atmospheric conditions was also studied. It was demonstrated that ECL-1, ECL-2, ECL-3 and ECL-4 increased significantly in an oxygen-saturated atmosphere, whereas in a nitrogen atmosphere ECL-1 and ECL-2 decreased remarkably and ECL-3 and ECL-4 disappeared. The results suggest that O_2 can significantly enhance ECL-1 and ECL-2 and is necessary for the formation of ECL-3 and ECL-4.

Effects of potential scan rate, direction and range

The effects on ECL behaviour of different potential scan rates (10–200 mV/s at intervals of 10 mV/s) were studied. As shown in Fig. 6, with an increase in scan rate, the intensities of ECL-1 and ECL-2 tended to increase up to 160 mV/s. ECL-1 did not change significantly, while ECL-2 decreased slightly >160 mV/s. Moreover, ECL-1 and ECL-2 shifted to a more negative potential from 10 to 170 and from 10 to 200 mV/s, respectively.

When the initial scan direction was negative, ECL-1 and ECL-2 increased considerably, while ECL-3 and ECL-4 disappeared. The results suggest that ECL-1 and ECL-2 might be enhanced by the species generated on the negative potential scan, whereas the species generated during the positive potential scan could be crucial to ECL-3 and ECL-4. If the initial scan direction

DOI: 10.1002/bio

was negative, OOH^- would be produced at a negative potential (27). Then, upon the reverse scan, OOH^- would be further oxidized to $O_2^{\cdot-}$, which could increase the intensity of ECL-1 and ECL-2. If the initial scan direction was positive, in the presence of O_2, BrO^- generated by the oxidation of Br^- on the positive scan and Br_2 generated during corresponding reverse scan, would play an important role for the formation of ECL-3 and ECL-4, respectively.

When the negative potential was fixed at –1.49 V and the positive potential was selected from 1.61 to 0.91 V at intervals of 0.1 V on the positive scan, ECL-3 and ECL-4 decreased from 1.61 to 0.91 V, and disappeared with a reversal potential <0.91 V, cvp5 and ECL-2 were not detected with a switching potential <0.91 V (before cvp3), which suggests that electrochemical or chemical reactions after cvp2 (>0.91 V) are related to the ECL-2, ECL-3 and ECL-4 reactions. Studies on the effect of Br^- demonstrated that ECL-2, ECL-3 and ECL-4 were related to Br^-. The results show that BrO^- was produced at a potential of >0.91 V. On the negative scan, when the positive potential was fixed at 1.61 V and the negative potential was selected from –0.89 to –1.49 V with an interval of 0.1 V, ECL-1 and ECL-2 were significantly enhanced. This further confirmed that the species generated on the negative scan are advantageous to ECL-1 and ECL-2.

Effects of pH

The effects of the pH on luminol ECL were investigated in the pH range of 5.6–13.0. Typical $I_{ECL} - E$ curves of luminol are shown in Fig. 7. It seems that all ECL peaks were related to the pH values of the luminol solutions. When the pH was <5.6, ECL-1, ECL-2, ECL-3 and ECL-4 were almost undetectable. Above pH 5.6, ECL-1 and ECL-2 increased significantly with an increase in pH, and reached a maximum at pH 10.6 and 9.6, respectively, then decreased sharply. This decrease might be due to more hydroxide ions on the electrode at higher pH interfering with the absorption of luminol (2). ECL-1 at pH 10.6 was enhanced by about two orders of magnitude compared with pH 7.0 and 13.0. ECL-3 and ECL-4 changed with pH irregularly. The position, number and shape of ECL peaks also changed with the pH of the solution. ECL-1 shifted negatively from pH 8.6 to 13.0. ECL-2 broadened above pH 9.6 and divided into two at pH 10.6, and vanished at pH 12.0. Moreover, the reproducibility of ECL became poor over pH 10.6. These changes could be due to the surface state of the electrode, solubility and activity of silver-containing compounds and some species generated in the electrochemistry process which could change with pH. The results suggest that a strong luminol ECL can be obtained on a silver nanoparticle self-assembled electrode both in neutral and alkaline solutions.

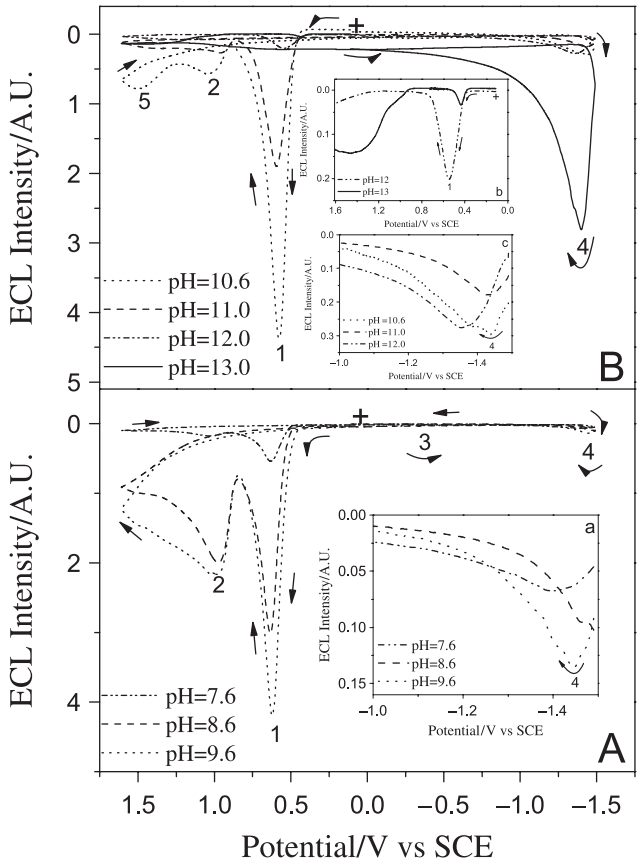

Figure 7. Effect of pH values on luminol ECL signals on a silver nanoparticle self-assembled gold electrode. pH = 5.6–10.0 PBS, 0.1 mol/L; pH = 10.0–13.0 NaOH medium; NaBr, 0.1 mol/L; luminol, 1×10^{-4} mol/L; scan rate, 40 mV/L; high voltage, –280 V. Inset (b) shows the enlarged ECL-1 from 0.11 to 1.60 V; insets (a) and (c) show the enlarged ECL-4 from –1.49 to –1.00 V.

Effects of buffer solutions

Several buffer solutions, such as KH_2PO_4–K_2HPO_4 (PBS), K_2HPO_4–citric acid (PCS) and citric acid–NaOH (CSS), were used in the luminol system on a silver nanoparticle self-assembled gold electrode in neutral solution under air-saturated conditions, as shown in Fig. 8. The intensities of ECL-1 and ECL-2 in CSS were about 20 and 12 times stronger than those in PBS or in PCS, respectively. The enhancement in CSS might be because citric acid was a good protecting agent for the nanoparticles (28). Moreover, in CSS, ECL-1 shifts to a more negative potential while ECL-2 shifts to a more positive potential, and they are well separated. The differences between PBS and PCS were minimal.

Effects of luminol concentration

The effects of luminol concentration (range 1×10^{-10}–10^{-4} mol/L at pH 7.0 and pH 8.0) on the ECL intensity were studied. It was found that the intensity of all ECL

DOI: 10.1002/bio

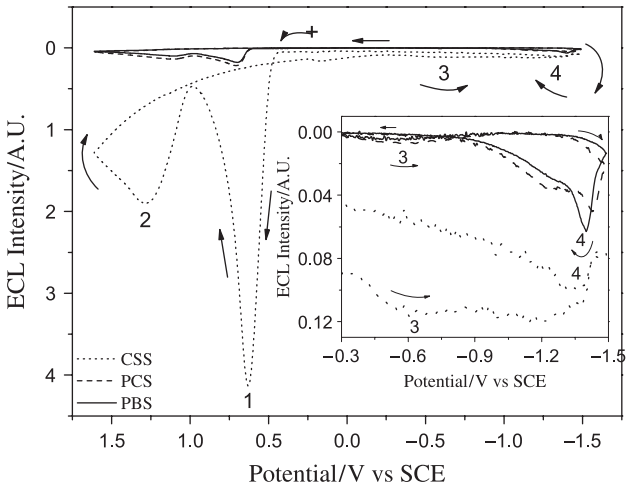

Figure 8. Effect of buffer solutions on luminol ECL signals on a silver nanoparticle self-assembled gold electrode. NaBr, 0.1 mol/L; luminol, 1×10^{-4} mol/L; scan rate, 40 mV/s; high voltage, –450 V. The inset shows the enlarged ECL-3 and ECL-4 from –0.30 to –1.49 V.

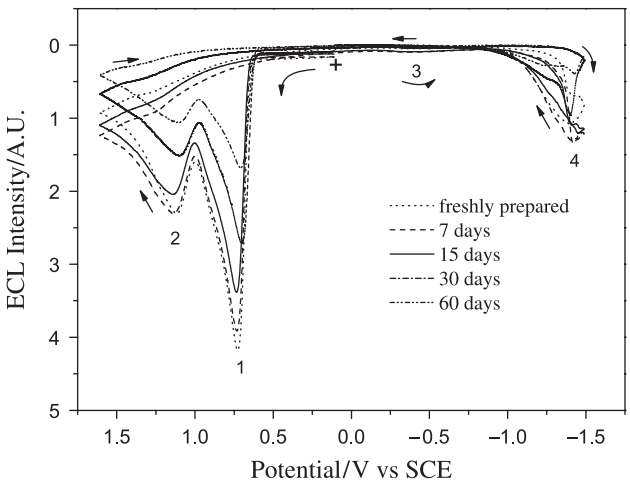

Figure 9. $I_{ECL} - E$ curves on a silver nanoparticle self-assembled gold electrode freshly prepared (dotted line) and stored for 7 days (dashed line), 15 days (solid line), 30 days (dashed/dotted line) and 60 days (dash/dot/dot line). pH 7.0 PBS, 0.1 mol/L; NaBr, 0.1 mol/L; luminol, 1×10^{-4} mol/L; scan rate, 40 mV/s; high voltage, –550 V.

peaks increased with an increase in luminol concentration, indicating that all ECL peaks depended on luminol. Moreover, the intensity of ECL-1 of luminol measured at pH 7.0 was found to be linear with the concentration of luminol in the range 1×10^{-9}–1×10^{-4} mol/L; the linear equation is $y = 42.561x + 4.788 \times 10^{-6}$, and the correlation coefficient is 0.998, where x is the concentration of luminol and y is the intensity of ECL-1. The lowest detectable luminol concentration (1×10^{-9} mol/L) is one order of magnitude lower than that on a gold nanoparticle-modified electrode. At pH 8.0, the intensity of ECL-1 was linear with the luminol concentration in the range 1×10^{-10}–1×10^{-7} mol/L; the linear equation is $y = 1009.118x + 2.973 \times 10^{-5}$, and the correlation coefficient is 0.997. The lowest detectable luminol concentration (1×10^{-10} mol/L) at pH 8.0 is comparable with that on a gold nanoparticle-modified electrode. Moreover, with an increase in pH value, the detectable concentration of luminol decreased further. The results demonstrate that luminol has a good emission efficiency and low detection limit in neutral and alkaline solutions on a silver nanoparticle self-assembled gold electrode and the detection limit of luminol at pH 7.0 is improved about a order of magnitude compared with that at pH 7.0 on a gold nanoparticle-modified electrode.

ECL stability and reproducibility on silver nanoparticle self-assembled gold electrode

Good stability and reproducibility of a gold nanoparticle self-assembled gold electrode in luminol system were found in our previous work (12). Stability and reproducibility of luminol ECL on a silver nanoparticle self-assembled gold electrode were also studied without any pretreatment, as shown in Fig. 9. Compared with the freshly prepared nanosilver-modified electrode, the intensity of ECL-1 on the nanosilver-modified electrode stored for 7, 15, 30 or 60 days decreased by ~5.8%, 18.3%, 34.5% or 59.5%, respectively. The intensity of ECL-2 decreased by ~0.4%, 11.6%, 34.1% or 55.1%, respectively. ECl-3 was too weak to compare. The intensity of ECL-4 changed by ~+19.1%, +10.1%, –10.5% or –63.9%, respectively. The silver nanoparticle self-assembled gold electrode could be used for at least a week without obvious changes in ECL intensities. Moreover, none of the CV curves changed significantly with time. It seems that a silver nanoparticle-modified electrode is not as stable as a gold nanoparticle-modified electrode. However, on a bare bulk gold electrode, the stability and reproducibility of luminol ECL signals were very poor, even when the pretreatment of the electrode was controlled rigorously. The results showed that the stability and reproducibility of ECL on the electrode in luminol were still good. The repulsive electrostatic forces could also keep the silver nanoparticles on the surface of the electrode from aggregation (29).

ECL spectra of various ECL peaks

The four peaks of ECL-1–ECL-4 were strong on a silver nanoparticle self-assembled gold electrode. ECL-5 occurred at 1.49 V at pH 10.6 NaOH solution. Therefore, the spectra of ECL-1, ECL-2, ECL-3, ECL-4 and ECL-5 on silver nanoparticle self-assembled electrode were analysed under air-saturated conditions, using a fluorescence spectrometer, as shown in Fig. 10. The results showed that the maximum emission of the five

DOI: 10.1002/bio

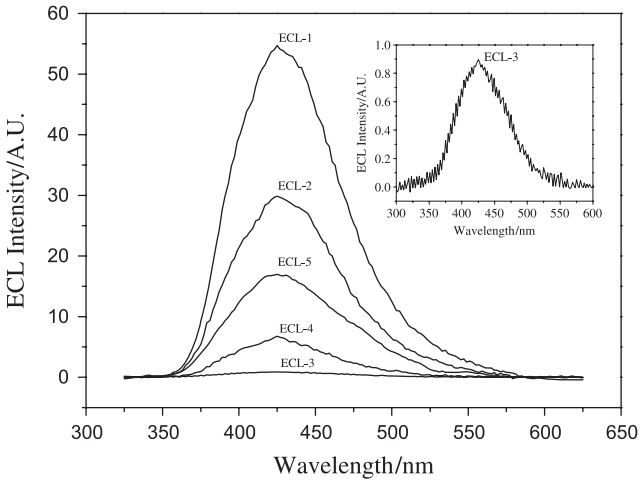

Figure 10. The CL spectra of luminol ECL peaks on a silver nanoparticle self-assembled gold electrode. NaBr, 0.1 mol/L; luminol, 1×10^{-4} mol/L; scan rate, 40 mV/s. ECL-1, ECL-2, ECL-3 and ECL-4 were measured in 0.1 mol/L pH 9.0 PBS, while ECL-5 was measured in pH 10.6 NaOH solution. Time recording for each ECL spectrum was 3 s; potential ranges for measuring ECL-1, ECL-2, ECL-3, ECL-4 and ECL-5 were 0.65–0.77 V, 1.06–1.18 V, –0.42 to –0.54 V, –1.43 to –1.31 V and 1.42–1.54 V, respectively. The inset shows the enlarged ECL-3 from 300 to 600 nm.

peaks was at 425 nm, corresponding to the light emission of 3-aminophthalate (1).

Mechanism of luminol ECL on silver nanoparticle self-assembled gold electrode

The ECL spectra indicated that 3-aminophthalate was the emitter of all ECL peaks. Thus, all ECL peaks were initiated by the reactions of luminol radical or luminol with the dissolved oxygen and various species generated at different potentials.

These studies revealed that ECL-1–ECL-4 of luminol on a silver nanoparticle self-assembled gold electrode depended on the same factors as on a gold nanoparticle self-assembled gold electrode. ECL-1, corresponding to cvp2, caused by the electro-oxidization of luminol anions to luminol radicals, could be enhanced by oxidative species such as O_2 and $O_2^{\cdot-}$. ECL-2, corresponding to cvp3, was induced by BrO^- oxidized from Br^-. ECL-3, corresponding to cvp7, was generated by the reaction of OOH^- reduced by dissolved oxygen in solution with luminol (4), and enhanced by nanosilver and BrO^-. ECL-4 appears to be related to Br_2 and OOH^-. If ECL-4 was only related to Br_2 and OOH^-, it should occur at less negative potentials. However, ECL-4 corresponded to the potential of H_2 onset. Thus, H formed at such high negative potentials might also take part in ECL-4 reactions. Moreover, nanosilver was also essential to the formation of ECL-4 because ECL-4 was not observed on a bare gold electrode. Therefore, ECL-4 might be caused by Br_2, OOH^-, H and nanosilver. Accordingly, the mechanism of luminol ECL-1–ECL-4 on a silver nanoparticle self-assembled gold electrode was similar to that on a gold nanoparticle self-assembled gold electrode (12).

ECL-5 occurred at 1.49 V at pH 10.6, which is unrelated to Br^- because, when $NaNO_3$ was used instead of NaBr or the concentration of NaBr was zero, ECL-5 still appeared. Moreover, ECL-5 did not depend on the electrode material, since similar oxidation waves were also observed on a paraffin-impregnated graphite electrode (4) and a gold electrode (7), respectively, at higher pH. It is well known that the reaction of luminol with O_2 or H_2O_2 can give weak chemiluminescence in the absence of catalysts. It was reported that OH^- at a higher pH was readily oxidized to OOH^- at higher positive potential and OOH^- could be further oxidized to $O_2^{\cdot-}$ (30). ECL-5 was likely due to the reaction of luminol radical anions with $O_2^{\cdot-}$.

In the presence of O_2, The pathways of all the luminol ECL peaks could be as follows:

ECL-1:

$$LH^- - e^- \rightarrow LH^{\cdot} \rightarrow L^{\cdot-} + H^+ \ (Ep = +0.73 \text{ V}) \quad (1)$$

$$L^{\cdot-} + O_2 \rightarrow O_2^{\cdot-} + L \quad (2)$$

$$L^{\cdot-} + O_2^{\cdot-} \rightarrow LO_2^{2-} \quad (3)$$

$$LO_2^{2-} \rightarrow AP^{2-*} + N_2 \quad (4)$$

$$AP^{2-*} \rightarrow AP^{2-} + h\nu \quad (5)$$

ECL-2:

$$Br^- + 2OH^- - 2e^- \rightarrow BrO^- + H_2O \ (Ep = +1.17 \text{ V}) \quad (6)$$

$$2L^{\cdot-} + 3BrO^- + 2OH^- \rightarrow 2AP^{2-*} + 3Br^- + H_2O + N_2 \quad (7)$$

ECL-3:

$$O_2 + H_2O + 2e^- \rightarrow OOH^- + OH^- \ (Ep = -0.45 \text{ V}) \quad (8)$$

$$LH^- + OOH^- + BrO^- \rightarrow AP^{2-*} + Br^- + H_2O + N_2 \quad (9)$$

ECL-4:

$$BrO^- + H_2O + e^- \rightarrow Br_2 + 2OH^- \quad (10)$$

$$H^+ + e^- \rightarrow H \quad (11)$$

$$LH^- + Br_2 + OOH^- + H + \text{nanosilver} \rightarrow AP^{2-*} + H^- + X + Y \quad (12)$$

where X and Y stand for the redox product of Br_2 and the other product, respectively.

DOI: 10.1002/bio

ECL-5:

$$3OH^- - 2e^- \rightarrow OOH^- + H_2O \quad (13)$$

$$OOH^- + OH^- - e^- \rightarrow O_2^{\cdot-} + H_2O \quad (14)$$

$$L^{\cdot-} + O_2^{\cdot-} \rightarrow AP^{2-*} \quad (15)$$

The experimental data indicate that ECL-1, ECL-2 and ECL-3 can be catalysed by silver nanoparticles. ECL reactions are considered to be a combination of electrode reactions and subsequent chemical reactions. There are two possibilities for the catalytic mechanism: first, the electrode reaction is catalysed by nanosilver via accelerating direct electron transfer between an electrode and the surrounding redox reactants; or second, the subsequent chemical reaction is catalysed. The higher current intensities of cvp2, cvp3 and cvp7 (Fig. 3A) on a silver nanoparticle self-assembled electrode were indicative of efficient electron transfer, therefore, the catalytic mechanism of ECL-1, ECL-2 and ECL-3 resulted from the electrocatalytic activity of the silver nanoparticle self-assembled electrode. ECL-1–ECL-3 on a silver nanoparticle-modified electrode was much stronger than that on a gold nanoparticle-modified electrode, which may be due to the faster electron transfer between the silver nanoparticle-modified electrode and the solution according to EIS (Fig. 2).

ECL-4 only occurred on a silver or gold nanoparticle-modified electrode and silver or gold nanoparticles took part in ECL-4. On a silver nanoparticle-modified electrode, ECL-4 is also stronger than that on a gold nanoparticle-modified electrode, which is likely because the reactivity of silver nanoparticles is better than that of gold nanoparticles (19).

CONCLUSIONS

Four luminol ECL peaks were found on a silver nanoparticle self-assembled gold electrode under conventional CV conditions in neutral and alkaline aqueous solutions. The mechanism for the four ECL peaks was proposed to be due to the reactions of luminol radical electro-oxidized by luminol or luminol with the dissolved oxygen and various electrogenerated species, such as HOO^-, BrO^-, Br_2 and H at different potentials, which was similar to that on a gold nanoparticle self-assembled electrode. Compared with a bulk gold electrode and a gold nanoparticle self-assembled electrode, the silver nanoparticle self-assembled gold electrode can significantly catalyse luminol ECL at both anode and cathode in neutral and alkaline solutions. Moreover, the silver nanoparticle self-assembled gold electrode can offer good stability and reproducibility and avoid tedious pretreatment of the electrode surface. The detection limit of 1×10^{-9} mol/L for luminol at pH 7.0 on a silver nanoparticle self-assembled electrode is obtained, which is one order of magnitude lower than that on a gold nanoparticle self-assembled electrode. The present study indicates that the silver nanoparticle self-assembled electrode is advantageous for luminol ECL, and has potential for sensitive detection of biologically important compounds at physiological pH using luminol as a label.

Acknowledgements

The support of this research by the National Natural Science Foundation of the People's Republic of China (Grant Nos. 29875025 and 20375037) and the Overseas Outstanding Young Scientist Program of the Chinese Academy of Sciences are gratefully acknowledged.

REFERENCES

1. Fähnrich KA, Pravda M, Guibault GG. Recent applications of electrogenerated chemiluminescence in chemical analysis. *Talanta* 2001; **54**: 531–559.
2. Sakura S. Electrochemiluminescence of hydrogen peroxide–luminol at a carbon electrode. *Anal. Chim. Acta* 1992; **262**: 49–57.
3. Lin XQ, Sun YG, Cui H. Potential-resolved electrochemiluminescence of luminol in alkaline solutions at glassy carbon and Pt electrodes. *Chin. J. Anal. Chem*. 1999; **27**: 497–503.
4. Cui H, Zou GZ, Lin XQ. Electrochemiluminescence of luminol in alkaline solution at a paraffin-impregnated graphite electrode. *Anal. Chem*. 2003; **75**: 324–331.
5. Kulmala S, Ala-Kleme T, Kulmala A, Papkovsky D, Loikas K. Cathodic electrogenerated chemiluminescence of luminol at disposable oxide-covered aluminium electrodes. *Anal. Chem*. 1998; **70**: 1112–1118.
6. Yoshimi Y, Sakai K. Analysis of reaction of luminol at an indium–tin oxide anode by cyclic voltammetry. *J. Chem. Eng. Jpn* 1997; **30**: 535–538.
7. Cui H, Zhang ZF, Zou GZ, Lin XQ. Potential-dependent electrochemiluminescence of luminol in alkaline solution at a gold electrode. *J. Electroanal. Chem*. 2004; **566**: 305–313.
8. Yu HX, Cui H, Guo JZ. Multi-channel electrochemiluminescence of luminol at a copper electrode. *Luminescence* 2004; **19**: 212–221.
9. Lin MS, Jan BI. Determination of hydrogen peroxide by utilizing a cobalt (II) hexacyanoferrate-modified glassy carbon electrode as a chemical sensor. *Electroanalysis* 1997; **9**: 340–344.
10. Sato Y, Sawaguchi T, Mizutani F. Potential-dependent chemiluminescence of luminol on the gold electrode modified with ferrocenylalkanethiol self-assembled monolayer. *Electrochem. Commun*. 2001; **3**: 131–135.
11. Wang J, Chen GN, Huang JL. The enhanced electrochemiluminescence of luminol on the nickel phthalocyanine modified electrode. *Analyst* 2005; **130**: 71–75.
12. Cui H, Xu Y, Zhang ZF. Multichannel electrochemiluminescence of luminol in neutral and alkaline aqueous solutions on a gold nanoparticle self-assembled electrode. *Anal. Chem*. 2004; **76**: 4002–4010.
13. Liu X, Chen DM, He TJ, Liu FC. Effect of CTAB on the surface-enhanced Raman scattering of tetrakis (4-N-methylpyridyl) porphyrin. *Chin. J. Chem. Phys*. 2003; **16**: 176–180.
14. Yuasa M, Nagaiwa T, Kato M, Sekine I, Hayashi S. Electrochemical properties of metalloporphyrin–clay complex-modified electrode systems—investigation as oxygen sensors. *J. Electrochem. Soc*. 1995; **142**: 2612–2617.
15. Chang G, Zhang J, Oyama M, Hirao K. Silver-nanoparticle-attached indium tin oxide surfaces fabricated by a seed-mediated growth approach. *J. Phys. Chem. B* 2005; **109**: 1204–1209.

16. Tang DP, Yuan R, Chai YQ, Zhang LY, Dai JY, Liu Y, Zhong X. Potentiometric immunosensor based on immobilization of hepatitis B surface antibody on platinum electrode-modified silver colloids and polyvinyl butyral as matrices. *Electroanalysis* 2005; **17**: 155–161.
17. Purkayshtha A, Baruah JB. Some aspects of copper and silver colloids in silane activation. *React. Funct. Polym*. 2005; **63**: 177–183.
18. Muniz-Miranda M. SERS-active Ag/SiO_2 colloids: photoreduction mechanism of the silver ions and catalytic activity of the colloidal nanoparticles. *J. Raman Spectrosc*. 2004; **35**: 839–842.
19. Chen YH, Nickel U. Superadditive catalysis of homogeneous redox reactions with mixed silver–gold colloids. *J. Chem. Soc. Faraday Trans*. 1993; **89**: 2479–2485.
20. Hernandez NC, Graciani J, Marquez A, Sanz JF. Cu, Ag and Au atoms deposited on the alpha-Al_2O_3(0001) surface: a comparative density functional study. *Surface Sci*. 2005; **575**: 189–196.
21. Fang JH, Huang YX, Li X, Dou XM. Aggregation and surface-enhanced Raman activity study of dye-coated mixed silver–gold colloids. *J. Raman Spectrosc*. 2004; **35**: 914–920.
22. Pan SL, Rothberg L. Chemical control of electrode functionalization for detection of DNA hybridization by electrochemical impedance spectroscopy. *Langmuir* 2005; **21**: 1022–1027.
23. Fu YZ, Yuan R, Tang DP, Chai YQ, Xu L. Study on the immobilization of anti-IgG on Au-colloid modified gold electrode via potentiometric immunosensor, cyclic voltammetry, and electrochemical impedance techniques. *Colloids Surfaces B* 2005; **40**: 61–66.
24. Szymanska I, Radecka H, Radecki J. Electrochemical impedance measurements for the investigation of odorants interaction with thiol layer immobilized onto gold electrode. *Sensors Actuators B* 2001; **75**: 95–100.
25. Li F, Cui H, Lin XQ. Potential-resolved electrochemiluminescence of $Ru(bpy)_3^{2+}/C_2O_4^{2-}$ system on gold electrode. *Luminescence* 2002; **17**: 117–122.
26. Tu YF, Huang BQ, Guo WY, Chen J. Electrochemiluminescence of luminol in neutral medium. *Chin. J. Anal. Chem*. 2002; **30**: 729–731.
27. Vitt JE, Johnson DC, Engstrom RC. The effect of electrode material on the electrogenerated chemiluminescence of luminol. *J. Electrochem. Soc*. 1991; **138**: 1637–1643.
28. Brown KR, Fox AP, Natan MJ. Morphology-dependent electrochemistry of cytochrome *c* at Au colloid-modified SnO_2 electrodes. *J. Am. Chem. Soc*. 1996; **118**: 1154–1157.
29. Hu XY, Xiao Y, Chen HY. Adsorption characteristics of $Fe(CN)_6^{3-/4-}$ on Au colloids as monolayer films on cysteamine-modified gold electrode. *J. Electroanal. Chem*. 1999; **466**: 26–30.
30. De Bethune AJ, Swendeman-Loud NA. Table of standard aqueous electrode potentials and temperature coefficients at 25°C. In *Encyclopedia of Electrochemistry*, Hampel CA (ed.). Reinhold: New York, 1964.

DOI: 10.1002/bio